Assessment of low-order theories for analysis and design of shrouded wind turbines using CFD

Aniket C. Aranake, Vinod K Lakshminarayan and Karthik Duraisamy

PhD Candidate, 496 Lomita Mall, Stanford, CA, 94305, USA
Postdoctoral Fellow, 496 Lomita Mall, Stanford, CA, 94305, USA
Assistant Professor, University of Michigan, Department of Aerospace Engineering

E-mail: aniket@stanford.edu

Abstract. The use of a shroud around the rotor of a wind turbine has been known to augment the airflow through the rotor plane and hence result in improved performance. This work uses Computational Fluid Dynamics (CFD) to assess the validity of several simple theories which attempt to extend Betz theory to shrouded turbines. Two CFD models are employed and compared to predictions of previously published models. The first makes use of a fixed pressure-drop actuator disk, while the second incorporates the twist and chord distribution of the turbine blade as well as an airfoil polar using a technique much like the classical blade element momentum (BEM) method. Calculations are performed for a sweep of turbine loadings using the fixed pressure-drop model and a sweep of tip speed ratios using the BEM model for both an open and shrouded turbine. Power is computed using a control volume approach for the fixed pressure-drop model and by integrating tangential forces for the BEM model. Information including mass flow ratio, power coefficient ratio, axial induction, and shroud force is extracted from the solution fields and compared against the predictions of low-order theories. Finally, the blade element model is used to redesign the turbine twist distribution to achieve greater performance across a range of tip speed ratios.

1. Introduction

Shrouded turbines, or diffuser augmented wind turbines (DAWTs), promise greater power extraction and lower cut-in speeds than conventional wind turbines. Few researchers have examined the benefits and economics of placing a diffuser around a wind turbine. A survey including a comprehensive history of shrouded turbines has been recently published by van Bussel [1]. Researchers have come to an agreement that there is significant potential for improvements in this concept. Realizing this potential not only requires improved understanding of the fine details of the flow physics using experiments and high-fidelity computational studies, but also development of low-order models that can provide quick assessment of a design as well as physical insight.

Low-order theories extending Betz theory to shrouded turbines rely on a considerable number of assumptions, and their usefulness to a designer relies on an understanding of how well these assumptions reflect reality. Presently, high-quality experimental data is not widely available for shrouded turbines for validation, though even if it were, experimental data would only reveal the total error of the theory due to all assumptions. Instead, a series of computational models with increasing fidelity can relax these assumptions in a stepwise manner. This provides a technique for assessing the relative error of each assumption.

Previous work by present authors [2, 3] have used high-fidelity three-dimensional RANS calculations including a transition model [4] to examine shrouded turbine flows in detail. In this work, two computational fluid dynamics (CFD) models obtained by simplifying the model from the earlier work are used to perform numerical experiments against which low-order theories are

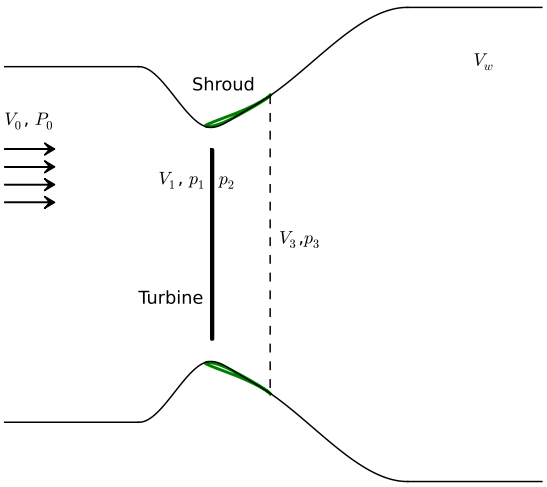

Figure 1. Streamtube for shrouded turbine

compared. When possible, the results are also compared with the predictions from the high-fidelity calculation. Finally, one of these models is used to design blades for a shrouded wind turbine.

2. Review of low-order models

The low-order models considered in this work are based on momentum theory using the actuator disk model. These models are attempts to extend Betz theory, the classical first approximation of the performance of a wind turbine, to the problem of shrouded turbines [1, 5, 6, 7]. In Betz theory, the rotor is represented by an infinitely thin disk. A fluid parcel passing through this disk experiences a discontinuous pressure drop by a fixed amount Δp while its velocity remains unchanged. The flow is assumed inviscid and incompressible. Furthermore, the flow is *quasi-1-dimensional*; velocity and pressure vary only in the axial direction and are assumed to be constant radially within the rotor streamtube. Under these assumptions, a control volume analysis leads to approximations for coefficients of both thrust and power based on a single parameter a, the axial induction factor [8], defined by

$$V_1 = V_0(1 - a). \tag{1}$$

Unlike for an open turbine, the upstream capture area of the streamtube for a shrouded turbine is larger than the rotor area (see Figure 1). At this level of model fidelity, no distinction is made between the rotor area and the streamtube area at the rotor plane; the rotor is assumed to extend to the inner wall of the shroud.

Under the actuator disk assumptions, the power extracted by a turbine is

$$P = TV_1, \tag{2}$$

or, in terms of coefficients,

$$C_P = C_T \frac{V_1}{V_0} \tag{3}$$

where V_0 is the windspeed and V_1 is the velocity at the actuator disk.

In the case of an open turbine, the velocity ratio appearing in Equation 3 is parameterized by the axial induction factor a. For a shrouded turbine, the situation is complicated by the fact that the shroud exerts a significant influence on the velocity field; the ratio V_1/V_0 depends not only on the properties of the turbine but also on the shape and size of the shroud.

Model I

One observation, first shown by Hansen et al. [6], is that for a given windspeed V_0 and thrust coefficient C_T,

$$\frac{C_{P,s}}{C_{P,o}} = \frac{V_{1,s}}{V_{1,o}} = \frac{\dot{m}_s}{\dot{m}_o} \tag{4}$$

where the subscripts s and o indicate shrouded and open turbines respectively. This identity shows that the extent to which a shroud increases the power output for a given turbine is the extent to which it increases the mass flow rate through the turbine.

Model II

The velocity ratio in Equation 3 is also constrained by the balance of momentum in the streamtube, given by

$$T + F_s = \rho A V_1 (V_0 - V_w), \tag{5}$$

where F_s is the force exerted on the shroud in the axial direction. Werle et al. [7] choose to nondimensionalize this force by the thrust, defining a shroud force coefficient C_s by

$$F_s = C_s \Delta p A \tag{6}$$

Applying this to Equation 3 along with the Bernoulli equation, yields the expression

$$C_P = \frac{1}{2} C_T (1 + C_s) \left(\sqrt{1 - C_T} + 1 \right). \tag{7}$$

This expression provides a means for computing power if both the turbine loading and the shroud force are known.

Model III

Another approach to evaluate the power coefficient comes from Jamieson [5], who derives an expression involving the turbine induction a as well as the induction at the rotor plane of an empty shroud, a_0. Rather than involve the shroud force, this approach posits that for a given shroud the wake velocity is related to the induction by a function f, as in

$$V_w = V_0 (1 - f(a)). \tag{8}$$

With this definition, the power coefficient becomes

$$C_P = (1 - a) \left(2 f(a) - f(a)^2 \right). \tag{9}$$

The function $f(a)$ is unknown, but it must satisfy two conditions:

- In this absence of a turbine, $V_0 = V_w$, and $f(a) = 0$.
- When the flow is fully blocked, $V_1 = 0$, $a = 1$, and $f(a) = 2$.

One possible form of f that satisfies these constraints is

$$f(a) = \frac{2(a - a_0)}{1 - a_0}, \tag{10}$$

where a_0 is the axial induction factor in the absence of a turbine. This leads to the following expression for power coefficient (See [5] for details).

$$C_p = \frac{4(a - a_0)(1 - a)^2}{(1 - a_0)^2}, \tag{11}$$

or, in terms of loading instead of induction,

$$C_P = \frac{1}{2} C_T (1 - a_0) \left(\sqrt{1 - C_T} + 1 \right). \tag{12}$$

While Equation 7 makes no assumptions beyond those of Betz theory, it relies on the shroud force coefficient C_s which is in general unknown. In contrast, Equations 11 and 12 rely only on a_0, which can be measured once for a given shroud then applied for all loading conditions. The cost of this advantage is that it was necessary to assume a form for the function f, and the appropriateness of this assumption is so far unknown.

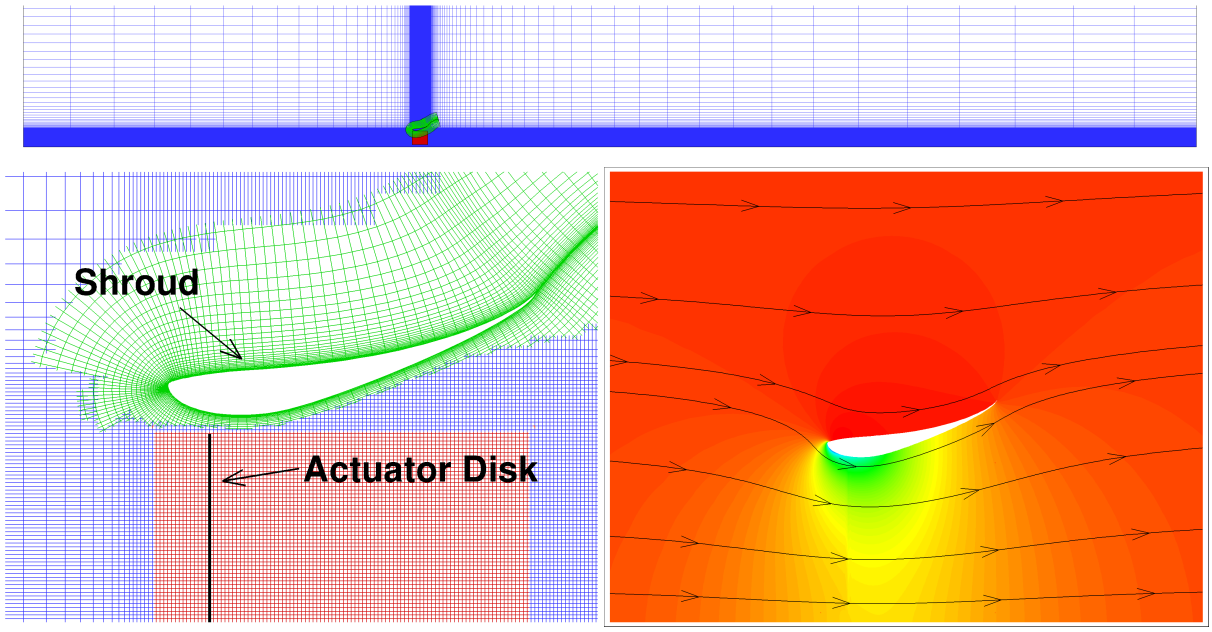

Figure 2. Grids used for computations. (Top) The grid dimensions are 205×160 for the background mesh, 101×88 for the blade mesh, and 171×31 for the shroud mesh in the wrap-around and normal directions respectively. The background mesh extends from $-25R$ to $50R$ in the axial direction and from 0.001 to $10R$ in the radial direction. In the blade mesh, the turbine is represented by 81 points, and the resolution of the nearby cells is $0.01R \times 0.01R$. (Left) A close-up of the shroud and blade meshes showing the hole-cutting. (Right) Pressure contours and streamlines from a sample solution (Fixed Δp, $C_T = 0.3$)

Model IV

One more approach to developing momentum theory for shrouded turbines is that of van Bussel [1]. This approach makes use of a concept of "extra back pressure," creating a distinction between shrouds with trailing edges parallel to the wind and shrouds with trailing edges angled so that flow exiting the shroud continues to expand for some distance downstream. Quantifying this extra back pressure with a higher fidelity model such as CFD relies on a number of modelling assumptions about how the shroud geometry is altered between the two operating conditions. This model is not considered in the present study.

3. CFD methodology

Flow solver

The compressible overset RANS solver OVERTURNS [9] has been previously validated in detail for the high-fidelity simulation and rotorcraft flows [10, 11, 12], and it has been used by present authors for the simulation of shrouded [2, 3] and open rotor turbine [4] flows. A third-order MUSCL approach with Koren's limiter [13] with Roe's flux difference splitting [14] was used for the convective terms, and the source terms were considered piecewise constant. Turkel preconditioner [15] is used to improve convergence and accuracy at low Mach numbers. At the rotor disk, the axial momentum and energy equations were modified to include the effect of a piecewise constant force with the magnitude. The overset mesh system used for simulations as well as a sample result are shown in Figure 2. An implicit hole-cutting technique developed by Lee [16] and improved by Lakshminarayan [9] is used to determine the connectivity information between various overlapping meshes. A sample case was run with double the mesh resolution near the turbine blade, and the performance parameters C_P and C_T were found to vary by less than 2%.

Simplified CFD models

In the present work, this flow solver is used to solve the steady axisymmetric Euler equations through an actuator disk. The momentum and energy equations at the location of the disk are augmented by source terms which represent a force acting on the flow and work done on the flow by the turbine. Two actuator disk models, referred to as "fixed Δp" and "BEM" are implemented and examined. The first and simpler model specifies a constant pressure drop at the disk location. With this technique, the thrust coefficient is essentially specified, since,

$$C_T = \frac{T}{\frac{1}{2}\rho V_0^2 A} = \frac{\Delta p}{\frac{1}{2}\rho V_0^2}. \tag{13}$$

To compute power, information about the turbine streamtube, defined as the set of streamlines passing through the turbine (depicted in Figure 1) is extracted from CFD solutions as a post-processing step. First, the mass flow through the turbine is computed by numerical integration at the turbine plane. Then, numerical integration is used to determine the radial extents of the streamtube at each axial location. Once the extents of the streamtube are determined, the power is computed using a control volume approach, i.e.,

$$C_P = \frac{\int_{A_0} \rho E u dA - \int_{A_w} \rho E u dA}{\frac{1}{2}\rho V_0^3 A}. \tag{14}$$

The second CFD model improves the representation of the turbine by using a strategy similar to the classic blade element momentum (BEM) model to determine the thrust and torque at each radial location. At each iteration, for each spanwise location, the lift and drag are computed using the local velocity and tabulated experimental data [17] for an S809 airfoil with the twist and chord distributions of the NREL Phase VI turbine [18]. Additional losses due to three-dimensionality were accounted for using Prandl's tip correction [8]. These lift and drag components are then projected onto the normal and tangential axes and summed up to compute power and thrust. In this case, unlike for the fixed Δp model, the turbine tip speed ratio, λ, is specified as an input and the thrust coefficient is computed by the simulation. Compared to low-order theory, the fixed Δp assumes the flow is axisymmetric rather than quasi-1-dimensional. The BEM model additionally incorporates a radial load distribution via a more realistic turbine description.

4. Results

As a first step, a series of open rotor cases are used to validate the implementation of the actuator disk models. In Figure 3, the computed thrust and power coefficients are compared to those from the classical result from Betz theory,

$$C_P = \frac{1}{2} C_T \left(1 + \sqrt{1 - C_T}\right). \tag{15}$$

The agreement between the computed and theoretical results at low loading are quite good for fixed Δp. For the BEM method, values corresponding to low tip speed ratios lie along the theoretical curve, whereas at higher tip speed ratios, there is considerable difference between the models. At these high tip speed ratios, the angle of attack, α, on some portions of the blade is such that a negative tangential force, F_t, is produced; some parts of the blade work against the rotation and contribute negatively to C_P. Figures 4 and 5 show force diagrams for both the normal condition and reversed force conditions. The sectional drag, which does contribute to F_t, is omitted from this diagram as its magnitude is small compared to lift.

Identical sweeps for both models were also performed for a shrouded configuration using a Selig S1223 airfoil for the shroud geometry. The length of the shroud is equal to the turbine radius. To assess the low-order developed by Hansen et al. [6] (model I), the ratios appearing on the left and right hand sides of Equation 4, $C_{P,s}/C_{P,o}$ $\dot{m}_s/\dot{m}_o$ are computed using fixed Δp model, and plotted against thrust coefficient in Figure 6. Interestingly, not only do the ratios appear to be equal as predicted by the equation, but the ratios remain nearly fixed as turbine thrust increases. This result differs from the original calculation performed by Hansen et. al [6], in which the ratio increased with increased turbine loading. Nevertheless, the plot confirms the prediction of Equation 4.

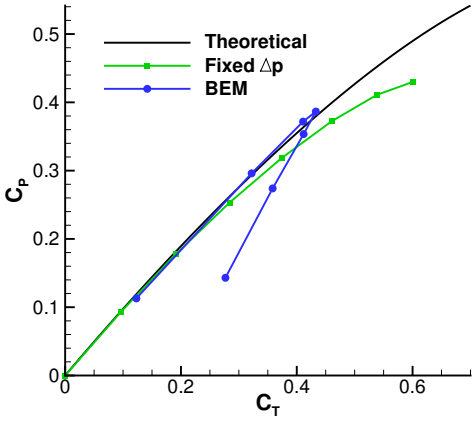

Figure 3. Constant pressure drop actuator disk model validation for open turbines. The theoretical curve comes from Equation 15.

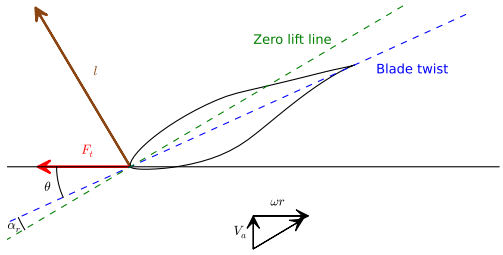

Figure 4. Normal operating condition.

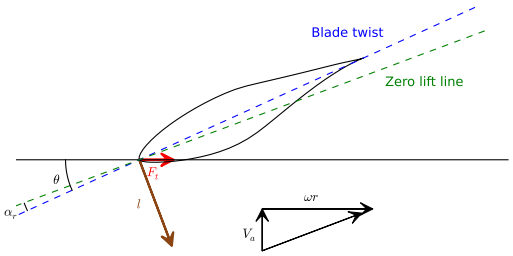

Figure 5. Reversed flow condition

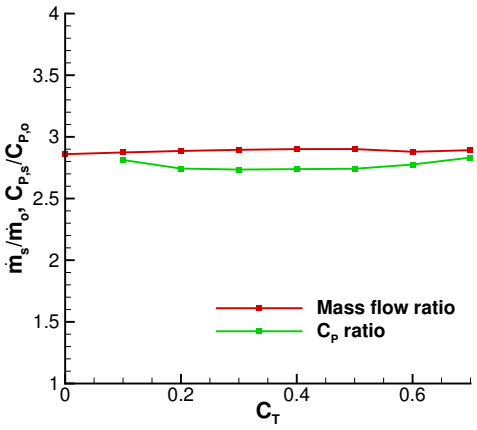

Figure 6. Ratios of mass flow rate and power coefficient using the fixed Δp model

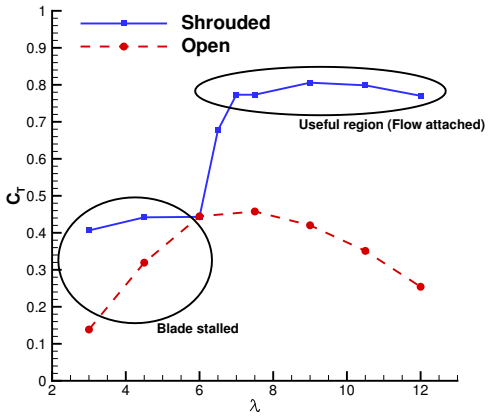

Figure 7. Thrust coefficients computed using BEM method. In regions where flow is not stalled, C_T is very different for the shrouded and unshrouded cases.

The BEM method provides a way of assessing the utility of Equation 4 in a more realistic setting. The derivation of this relation relies on the assumption that if a turbine is placed inside a shroud, its thrust coefficient is unaffected. In reality, the flow augmentation due to the shroud leads to significantly higher loadings. Figure 7 plots C_T for a sweep of tip speed ratios for both an open and shrouded turbine. At low tip speed ratios, the assumption that the C_T remains constant between the open and shrouded settings is reasonable, but at these speeds the turbine blade is stalled across its entire span. At higher tip speed ratios, where the local angles of attack

along the blade are in the useful region of the airfoil's polar, the effect of the shroud leads to thrusts beyond the range of thrusts achieved by the bare turbine.

Next the low-order model developed by Werle et al. [7] (model II) is assessed. Equation 7 provides a technique for computing C_P assuming the shroud force coefficient C_s is known. In his paper, Werle suggests that C_s remains constant with varying C_T, an assumption that allows the use of Equation 7 to compute the power coefficient once C_s is known for a single condition. In general, however, C_s is an unknown function of both the shroud geometry and C_T. Indeed, the definition of C_s as given in Equation 6 requires that $C_s \to \infty$ as $C_T \to 0$. Figure 8 plots C_s against C_T for the present sweep of CFD cases. As defined by Equation 6, C_s decreases with increasing turbine loading. For comparison, a more traditional nondimensionalization for shroud force is also shown. Figure 8 shows that C_s varies considerably with loading. Additionally, the BEM model reveals that the fixed Δp model in general overpredicts the shroud force for a given turbine loading in the useful operating regions.

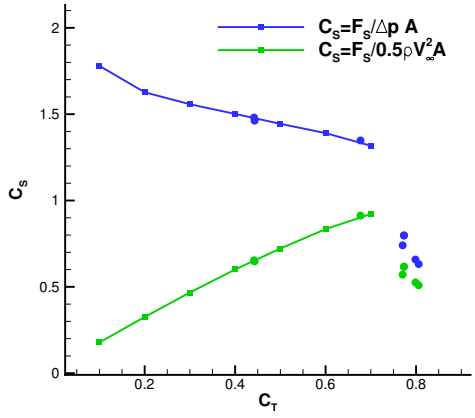

Figure 8. Shroud force coefficient C_s. The lines in this plot are computed using the fixed Δp method. The circles are from the BEM method.

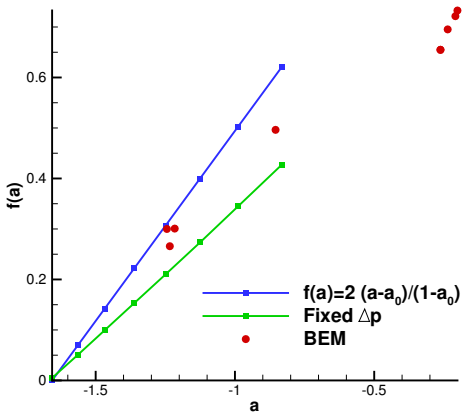

Figure 9. The function $f(a)$ extracted from CFD and its assumed form.

Next the low-order model of Jamieson [5] (model III) is assessed. Equation 10 makes a prediction about the wake velocity of a shrouded turbine based on the induction at the rotor plane. The quantities a and a_0 are extracted from CFD results by computing average velocities within the turbine streamtube and using Equation 1. The result is plotted in Figure 9. The function $f(a)$ is also extracted for both the fixed Δp and the BEM methods and is plotted along side the curve of Equation 10. In general, the assumed form of this equation overestimates the function $f(a)$, i.e., it underestimates the wake velocity. It is worth noting that scaling the expression for $f(a)$ of Equation 10 by a constant violates the second condition listed above.

From CFD solutions, it is possible to extract several of the quantities appearing in Equations 7, 9, 11, and 12. Figure 10 plots the directly computed C_P against C_T alongside curves from these equations. The small discrepancy seen between the fixed Δp calculations, Equation 7, and Equation 9 are due to numerical errors which accumulate between the CFD and post-processing steps used to extract C_s, a, and $f(a)$ from the solutions.

A larger discrepancy appears in Figure 10 for Equations 11 and 12. The large portion of the error in these expressions is due to the fact that the form of the function $f(a)$ has been assumed and is not known exactly. Values of $f(a)$ extracted from the far wake of the CFD solutions are compared against values predicted by extracted values of a and a_0 using Equation 10 in Figure 9.

The BEM model, on the other hand, reveals that the fixed Δp model overestimates the power-thrust curve. This general trend is confirmed by the results of previously computed 3D RANS simulations. A possible explanation for this is that the fixed Δp actuator disk model

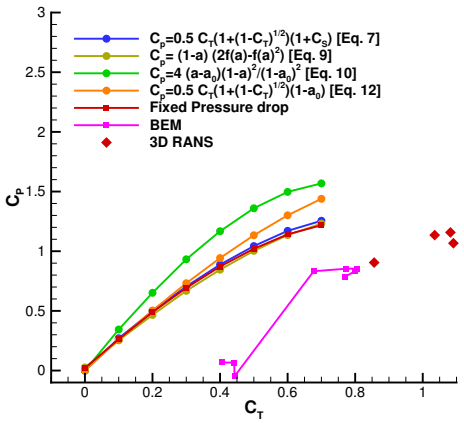

Figure 10. Pressure coefficient vs thrust coefficient. The fixed Δp model and low-order models overpredict all overpredict the C_p curve. The tip speed ratios for the BEM model are those shown in Figure 7. The tip speed ratios for the RANS calculations are $\lambda = 5.42$, $\lambda = 6.77$, $\lambda = 8.12$, and $\lambda = 10.8$. See [3]

assumes that all of the power removed from a wind turbine's streamtube is converted into useful power. In reality, the power loss defined by the right hand side of Equation 14 includes power extracted by creating torque on the rotor, the useful component, as well as work done on the fluid by the turbine thrust, which is not used to produce electricity. For this reason, the fixed Δp model represents an upper bound to the amount of power that can be achieved by any blade design for a given shroud.

5. Blade design using BEM

Models which use a fixed Δp assumption for the turbine have no knowledge of blade geometry and cannot be used for design. The BEM model, however, does incorporate blade geometry and is a convenient tool for the design of a shrouded turbine blade. This section considers the design of a wind turbine blade's twist distribution for operation for a shrouded turbine.

Modern turbines operate at variable speeds, so development of a single optimal design for annual energy production requires knowledge of how much time the turbine spends operating at each tip speed ratio. In practice this depends on many factors and will vary between turbines. If, however, it is satisfactory to assume that the turbine will spend much of its operating time at a single λ, then it is sufficient to optimize the C_P. In this case, the BEM model provides a convenient way to solve for the optimal blade twist distribution. At each iteration of the CFD solver, the blade tangential force coefficient is computed by

$$C_t = C_l \sin(\phi) - C_d \cos(\phi) \tag{16}$$

where C_l is the lift coefficient, C_d is the drag coefficient, and ϕ is the flow angle. This tangential force coefficient is the aerodynamic contribution to power. In the standard BEM approach, the angle of attack is computed using the twist and flow angle, $\alpha = \phi - \theta$. In order to design the twist distribution, this process is reversed. Rather than using a prescribed blade twist, the angle of attack α is selected to maximize Equation 16. This is a one-dimensional optimization problem and is solved using the golden section method. The bounds were set to $\alpha \in [0°, 12°]$, avoiding airfoil stall. Figure 11 shows the maximizing values of α along with the attained C_t for a range of flow angles. Once the optimal α is known, it is easy to solve for the optimal twist. By inverting the BEM method in this way, an optimal blade is designed as the CFD solver converges.

Optimal blades using this procedure have been designed for tip speed ratios ranging from $\lambda = 3$ to 7. Simulations with $\lambda > 7$ were attempted but were found not to converge. In these cases, the axial forces were so large that a control volume analysis predicts reversed flow downstream of the turbine. In partially converged solutions, these forces direct fluid around the shroud rather than through it. This appears to be the turbine thrust singularity for actuator disks which has been addressed by Werle [19] for low-order theory. Further investigation is required to determine whether the origin of this phenomenon is physical or numerical.

As shown in Figure 12, greater power coefficients are achieved at greater tip speed ratios within the range considered. Figure 13 shows the optimal twist distributions in these cases. For the purpose of comparison, the twist distributions have been offset so that the twist at the root is zero. At $\lambda = 3$, the optimal value assumes the top end of the bracket $\alpha = 12°$ across the entire region of the blade. As λ increases, starting at the blade tip, the optimal α moves away from this upper bound. This is due to a decrease in flow angle, as seen in Figure 11.

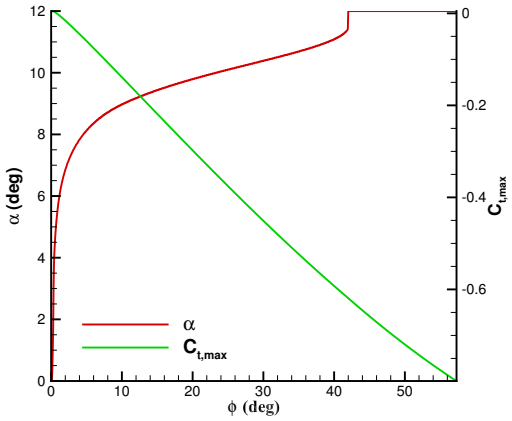

Figure 11. Angle of attack which maximizes C_t and maximum C_t attained as functions of the flow angle ϕ.

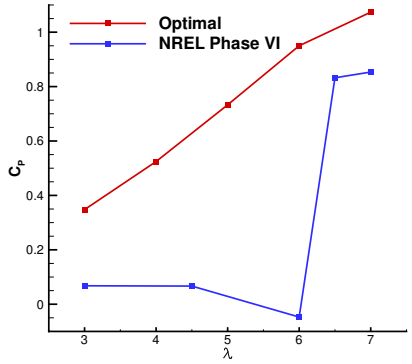

Figure 12. Performance coefficients for optimized blades along with original NREL Phase VI

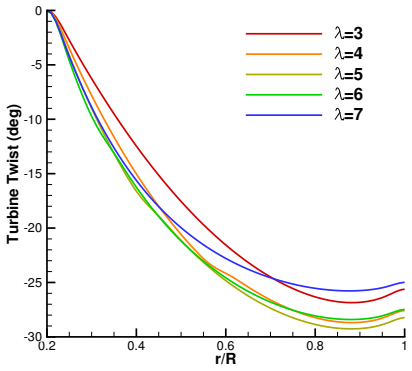

Figure 13. Twists distributions of optimized blades

6. Conclusions and Future Work

The success of a low-order theory for shrouded turbines should be measured by the extent to which the most relevant performance parameters of the system are well-predicted and by the extent to which the theory enhances a designer's understanding of the shrouded turbine system. The present work has summarized some of the theories previously published in literature and provided an assessment of their accuracy.

Two CFD models have been used to assess several low-order theories for the analysis of shrouded turbines. Based on this analysis, the following conclusions are drawn:

- The ratio of mass flow rate for a shrouded and open turbine is equal to that of the power coefficients according to the fixed Δp assumption, however in practice the thrust coefficient is significantly augmented in the shrouded case and the relationship no longer applies.
- The shroud force coefficient, regardless of choice of nondimensionalization, has strong dependence on the turbine loading even when assuming Δp is fixed.

- The assumed form of the far wake induction function given by Equation 10 overestimates $f(a)$.

The BEM model developed for analysis, which is more accurate than a fixed Δp model but considerably cheaper than a RANS simulation, finds additional utility in the problem of design. Optimal twist distributions for a range of tip speed ratios have been computed.

Based on the results of this study, the following items are proposed as future work:

- Continued development and improvement of low-order theories using comparison against higher-fidelity simulation to measure utility.
- Further investigation into using the BEM method for high thrust
- Coupled design of a shrouded turbine blade and shroud using the BEM model.
- Embedding the BEM model developed here in a multi-fidelity framework along with 3D RANS for optimization.

Acknowledgment

This work is supported by the DoD NDSEG fellowship and by the DoE ASCR program on Fluid/Structure interactions in Wind Turbine Applications at Stanford University. The authors would like to thank Sravya Nimmagadda for the original implementation of the BEM model.

[1] van Bussel, G., "The science of making more torque from wind: Diffuser experiments and theory revisited," *Journal of Physics: Conference Series*, Vol. 75, 2007.

[2] Aranake, A., Lakshminarayan, V., and Duraisamy, K., "Computational Analysis of Shrouded Wind Turbine Configurations," *51st AIAA Aerospace Sciences Meeting*, Dallas, TX, January 2013.

[3] Aranake, A., Lakshminarayan, V., and Duraisamy, K., "Computational Analysis of Shrouded Wind Turbine Configurations," *Renewable Energy*, To be published.

[4] Aranake, A., Lakshminarayan, V., and Duraisamy, K., "Assessment of Transition Model and CFD Methodology for Wind Turbine Flows," 42^{nd} *AIAA Fluid Dynamics Conference and Exhibit*, New Orleans, LA, June 2012.

[5] Jamieson, P., "Beating Betz: Energy Extraction Limits in a Constrained Flow Field," *Journal of Solar Energy Engineering*, Vol. 131, 2009.

[6] Hansen, M. O. L., Sørensen, N. N., and Flay, R. G. J., "Effect of Placing a Diffuser Around a Wind Turbine," *Wind Energy*, Vol. 3, 2000.

[7] Werle, M. J. and Presz Jr., W. M., "Ducted Wind/Water Turbines and Propellers Revisited," *Journal of Propulsion and Power*, Vol. 24, No. 5, 2008.

[8] Hansen, M. O. L., *Aerodynamics of Wind Turbines*, Earthscan, 2nd ed., 2008.

[9] Lakshminarayan, V. K., "Computational Investigation of Micro-Scale Coaxial Rotor Aerodynamics in Hover," *Ph.D. dissertation, Department of Aerospace Engineering*, 2009.

[10] Baeder, J., Duraisamy, K., and Lakshminarayan, V., "RANS Predictions of Complex Hovering Rotor Configurations: From Micro Scale to Full Scale," *Computational Fluid Dynamics Journal*, Vol. 18, No. 3-4, 2011.

[11] Lakshminarayan, V. K. and Baeder, J. D., "Computational Investigation of Microscale Shrouded Rotor Aerodynamics in Hover," *Journal of the American Helicopter Society*, 2011, 56, 042002.

[12] Duraisamy, K., Ramasamy, M., Baeder, J., and Leishman, G., "High Resolution Wake Capturing Methodology for Hovering Rotor Simulations," *Journal of the American Helicopter Society*, Vol. 52, No. 2, 2007.

[13] Koren, B., "Multigrid and Defect Correction for the Steady Navier-Stokes Equations," *Journal of Computational Physics*, Vol. 87, No. 1, March 1990, pp. 25–46.

[14] Roe, P., "Approximate Riemann Solvers, Parameter Vectors and Difference Schemes," *Journal of Computational Physics*, Vol. 43, No. 2, October 1981, pp. 357–372.

[15] Turkel, E., "Preconditioning Techniques in Computational Fluid Dynamics," *Annual Review of Fluid Mechanics*, Vol. 31, 1999, pp. 385–416.

[16] Lee, Y., "On Overset Grids Connectivity and Vortex Tracking in Rotorcraft CFD," *Ph.D. dissertation, Department of Aerospace Engineering*, 2008.

[17] Ramsay, R. R., Janiszewska, J. M., and Gregorek, G. M., "Wind Tunnel Testing of Three S809 Aileron Configurations for use on Horizontal Axis Wind Turbinesi : Airfoil Performance Report," *The Ohio State University*, , No. DE-AC36-83CH10093, 1996.

[18] Hand, M. M., Simms, D., Fingersh, L. J., Jager, D. W., Cotrell, J. R., Schreck, S., and Lawood, S. M., "Unsteady Aerodynamics Experiment Phase VI: Wind Tunnel Test Configurations and Available Data Campaigns," *NREL/TP-500-29955*, 2001.

[19] Werle, M., "Wind Turbine Wall-Blockage Performance Corrections," *Journal of Propulsion and Power*, Vol. 26, No. 6, 2010, pp. 1317–1321.